

Blind Channel Equalization Using Vector-Quantized Variational Autoencoders

Jinxiang Song, *Student Member, IEEE*, Vincent Lauinger, *Student Member, IEEE*,
 Yibo Wu, *Student Member, IEEE*, Christian Häger, *Member, IEEE*,
 Jochen Schröder, *Member, IEEE*, Alexandre Graell i Amat, *Senior Member, IEEE*,
 Laurent Schmalen, *Fellow, IEEE*, and Henk Wymeersch, *Senior Member, IEEE*

Abstract—State-of-the-art high-spectral-efficiency communication systems employ high-order modulation formats coupled with high symbol rates to accommodate the ever-growing demand for data rate-hungry applications. However, such systems are more vulnerable to linear and nonlinear transmission impairments, and it is important to mitigate the performance loss via digital signal processing. In this paper, we propose a novel machine learning approach for blind channel equalization and estimation using the vector quantized (VQ) variational autoencoder (VAE) framework. The proposed approach generalizes the applicability of the conventional VAE-based equalizer to nonlinear systems employing high-order modulation formats by introducing a codebook component and an associated novel loss function. We evaluate the performance of the proposed method over a linear additive white Gaussian noise channel with intersymbol interference and two nonlinear scenarios. Simulation results show that the proposed method can achieve similar performance as a data aided equalizer using the minimum-mean-squared-error (MMSE) criterion, and outperforms the blind constant modulus algorithm (CMA) and the VAE-based channel equalizer. Furthermore, we show that for the linear channel, the proposed scheme exhibits better convergence properties than the MMSE-based, the CMA-based, and the VAE-based equalizers in terms of both convergence speed and robustness to variations in training batch size and learning rate.

I. INTRODUCTION

The performance of communication systems is constrained by the linear and nonlinear distortions originating from hardware impairments and non-ideal communication channels.

This work was supported by the Knut and Alice Wallenberg Foundation under grant No. 2018.0090. The work of C. Häger was supported by the Swedish Research Council under grant No. 2020-04718. The work of V. Lauinger was funded by the German Federal Ministry of Education and Research under grant agreement 16KIS1316. The work of L. Schmalen was supported by the European Research Council (ERC) under the European Union's Horizon 2020 research and innovation program (grant agreement No. 101001899). (*Corresponding author: Jinxiang Song.*)

Jinxiang Song, Christian Häger, Alexandre Graell i Amat, and Henk Wymeersch are with the Department of Electrical Engineering, Chalmers University of Technology, 41296 Gothenburg, Sweden (emails: {jinxiang, christian.haeger, alexandre.graell, henkw}@chalmers.se).

Yibo Wu is with Ericsson Research, Ericsson AB, 41756 Gothenburg, Sweden, and also with the Department of Electrical Engineering, Chalmers University of Technology, 41296 Gothenburg, Sweden (e-mail: yibo.wu@ericsson.com).

Jochen Schröder is with the Department of Microtechnology and Nanoscience, Chalmers University of Technology, 41296 Gothenburg, Sweden (email: jochen.schroeder@chalmers.se).

Vincent Lauinger and Laurent Schmalen are with the Communications Engineering Lab (CEL), Karlsruhe Institute of Technology (KIT), 76131 Karlsruhe, Germany (email: {vincent.lauinger, laurent.schmalen}@kit.edu).

Such constraints become even more severe for high spectral-efficiency systems employing high-order modulation formats together with high symbol rates. To support the ever-growing demand for high-bandwidth services such as cloud computing, video streaming, and autonomous driving, it is crucial to mitigate the detrimental impact of transmission impairments that limit the systems' throughput.

Several receiver-side digital signal processing (DSP) techniques have been proposed for channel equalization in both wireless [1] and optical communications [2]. Conventionally, these algorithms either assume a channel model (e.g., a linear channel with memory [3], a nonlinear channel governed by the Manakov equation [4]) or specific statistical properties in the received signal (e.g., second-order statistics [5]). In the case where such assumptions do not hold or significantly deviate from the real scenarios, these algorithms may suffer from severe performance penalties. To circumvent these challenges, machine learning techniques have attracted much interest in recent years, with the aim to mitigate transmission impairments directly by learning from data. In particular, neural networks (NNs) have been successfully applied to equalize various nonlinear channels, showing promising performance [6]–[14].

In general, receiver side channel equalizers fall into two categories: data aided (or pilot-based) channel equalizers and blind channel equalizers. Data aided equalizers require the transmission of pilot symbols prior to data transmission, which decreases the overall system throughput, especially for dynamic or fast time-varying channels for which pilot symbols need to be transmitted periodically. Blind channel equalizers, on the other hand, do not require the transmission of pilot symbols and have the potential to achieve higher throughputs. Therefore, high-performance blind channel equalizers are preferable in many practical applications to achieve maximum spectral efficiency.

The most popular algorithm for blind adaptive channel equalization is the constant modulus algorithm (CMA) [15] and its variants, e.g., the modified CMA [16] and the multi-modulus algorithm [17]. The CMA was originally designed for linear channels and phase shift keying constellations and may suffer from poor convergence when the channel is nonlinear or introduces significant distortions [18]. Based on the constant modulus criterion, nonlinear equalizers based on NNs have been studied in [18]–[20], showing improved performance compared to their linear counterparts. Although the CMA is immune to phase noise and has low computational com-

plexity, it is modulation format dependent and suffers from phase ambiguity; reliable symbol detection is only possible when the CMA is used in combination with a carrier-phase recovery block [21]. The decision-directed least-mean-squares (DD-LMS) algorithm [22], [23] circumvents the modulation dependence of the CMA by switching to a decision-directed mode after proper equalizer pre-training [24].

As an alternative to the CMA-based blind channel equalizer, a different approach based on variational inference and the variational autoencoder (VAE) has been proposed in [25]. The VAE-based blind equalizer was originally proposed for linear systems employing 4-QAM, but has later been extended to cope with a nonlinear channel considering BPSK transmission [26]. However, the nonlinear channel under consideration assumes component-wise nonlinearity only (see [26, Eq. (2)]), and may not be able to accurately model the interplay between linear and nonlinear distortions that exist in many practical systems. In [27], the VAE-based equalizer was generalized to cope with high-order modulation formats coupled with probabilistic constellation shaping and shown to be more performant than the CMA-based equalizer over a polarization-multiplexed optical fiber channel. While [27] showed promising performance of the VAE-based equalizer, the approach assumes a linear dispersive channel, and the equalizer training requires a closed-form analytical solution of the evidence lower bound (ELBO) (see [25]–[27] for more details), which is only available for channels that can be described in a simple form (e.g., the linear additive white Gaussian noise (AWGN) channel considered in [25]–[27]). However, many practical communication scenarios, including communication over the optical fiber channel, and transmission with non-ideal hardware components (e.g., nonlinear power amplifiers (PAs), quantization-constrained receivers), cannot be accurately modeled in a simple form (e.g., as an AWGN channel). Consequently, the applicability of the VAE-based equalizer proposed in [25]–[27] is limited.

In this paper, we propose a novel blind channel equalizer based on a variant of the VAE, namely the vector quantized VAE (VQ-VAE) [28]. Compared to [25]–[27], training of our proposed method does not rely on the maximization of the ELBO and can be applied to both linear and nonlinear channels. It is noteworthy that in the machine learning literature, VQ-VAEs have been commonly used as generative models in fields like image, text, and audio generation. However, in the communication setup, there have been limited treatments of the VQ-VAE framework, with only a few notable exceptions: semantic communication [29] and joint source-channel coding [30]. For blind channel equalization, VQ-VAEs have never been considered before. The main contributions of this paper are as follows:

- 1) We propose a novel blind channel equalizer based on the VQ-VAE framework. The proposed method addresses a major shortcoming in previous works, in particular the requirement in [25], [27] that a closed-form expression for the ELBO is needed for the VAE-based equalizer training, and the fact that the nonlinear VAE in [26] is limited to BPSK transmission.
- 2) We conduct a thorough numerical study demonstrating

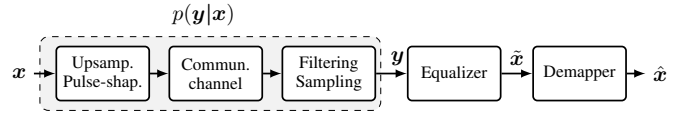


Fig. 1. The communication setup: discrete symbols \mathbf{x} are upsampled and filtered by a pulse-shaping filter prior to transmission over the considered channel. At the receiver, the channel output is pre-processed (i.e., filtering, resampling) before channel equalization. The equalizer output is then used for symbol demapping.

the effectiveness of the proposed method for both a linear AWGN channel and two nonlinear scenarios.¹ We show that for the linear and nonlinear channels under investigation, the proposed method can achieve similar performance as its data-aided counterpart while outperforming the reference blind channel equalizers.

- 3) We investigate the convergence behavior of our proposed equalizer for the linear channel, showing that the proposed method exhibits better convergence properties than the chosen baseline schemes.

The remainder of this paper is structured as follows. In Section II, we present our system model. In Section III, we start with a brief introduction to *variational inference* and the VAE. We then briefly describe the framework of VAE-based equalizers and its limitations. Section IV describes the proposed VQ-VAE-based blind channel equalizer and its associated cost function for training. In Section V and Section VI, detailed descriptions of our simulation setup as well as numerical results are presented. Finally, the paper is concluded in Section VII.

Notation: \mathbb{Z} , \mathbb{R} , and \mathbb{C} denote the sets of integers, real numbers, and complex numbers, respectively. We use boldface letters to denote vectors and matrices (e.g., \mathbf{x} and \mathbf{A}). $(\cdot)^\top$ and $(\cdot)^\dagger$ denote transpose and conjugate transpose, respectively. For a vector $\mathbf{x} = (x_1, \dots, x_n)^\top$, x_i denotes the i -th element of \mathbf{x} , $\|\mathbf{x}\|^2 = \sum_{i=1}^n |x_i|^2$ denotes the squared Euclidean norm. For a matrix \mathbf{A} , $(\mathbf{A})_i$ returns the i -th row of \mathbf{A} , and $(\mathbf{A})_{i,j}$ returns the element on i -th row and j -th column of \mathbf{A} . \mathbf{I}_n is the $n \times n$ identity matrix. $\mathcal{CN}(\mathbf{x}; \boldsymbol{\mu}, \boldsymbol{\Sigma})$ denotes the distribution of a proper complex Gaussian random vector with mean $\boldsymbol{\mu}$ and covariance matrix $\boldsymbol{\Sigma}$, evaluated at \mathbf{x} (\mathbf{x} may be omitted to represent the entire distribution). Lastly, $\mathbb{E}\{\cdot\}$ denotes the expected value.

II. SYSTEM MODEL

We consider the communication setup depicted in Fig. 1. Let $\mathbf{x} \in \mathcal{X}^N$ denote a vector of N baseband symbols sampled from a complex signal constellation $\mathcal{X} \subset \mathbb{C}$, with $M = |\mathcal{X}|$ denoting the cardinality of \mathcal{X} . The symbols are R -times upsampled and filtered by a pulse-shaping (PS) filter prior to transmission over a non-ideal communication channel. In this paper, we consider block transmission, and the channel is assumed to be time-invariant within one block. Furthermore, the channels under consideration are a linear AWGN channel

¹The complete source code to reproduce all results in this paper is available at <https://github.com/JSChalmers/VQ-VAE-based-equalizer>

with memory and two nonlinear channels, for which detailed configurations are provided in Section V and Section VI, respectively. At the receiver, the channel output is filtered and resampled to have K samples per symbol (SPS). The resulting observation vector is denoted by $\mathbf{y} \in \mathbb{C}^{KN}$. We remark that in this paper, the channel describes the transition from the discrete symbols \mathbf{x} to the observation vector \mathbf{y} , and is described by the conditional probability distribution $p(\mathbf{y}|\mathbf{x})$. We further assume that the channel law $p(\mathbf{y}|\mathbf{x})$ is governed by some underlying parameters $\boldsymbol{\theta}^*$, i.e., $p(\mathbf{y}|\mathbf{x}, \boldsymbol{\theta}^*)$, where $\boldsymbol{\theta}^*$ is omitted in the following for notation simplicity.

We focus on the problem of recovering the transmitted symbols \mathbf{x} from the channel observation \mathbf{y} , for which the optimal decision is given by the maximum a posteriori (MAP) criterion,

$$\hat{\mathbf{x}} = \arg \max_{\mathbf{x} \in \mathcal{X}^N} p(\mathbf{x}|\mathbf{y}) = \arg \max_{\mathbf{x} \in \mathcal{X}^N} \frac{p(\mathbf{y}|\mathbf{x})p(\mathbf{x})}{p(\mathbf{y})}, \quad (1)$$

where $p(\mathbf{x})$ is the prior distribution of the transmitted data \mathbf{x} , and $p(\mathbf{y})$ is the marginal distribution (also referred to as evidence) of the channel observations \mathbf{y} . In practice, applying exact MAP detection is challenging, as it requires searching over all M^N different possible input combinations, for which the computational complexity grows exponentially with the sequence length N and constellation order $M = |\mathcal{X}|$. Furthermore, the MAP detector requires accurate knowledge of the channel (i.e., $p(\mathbf{y}|\mathbf{x})$ must be fully known). Although reliable channel estimation can be obtained at the expense of using training sequences, we consider a different setup where no channel knowledge is available at the receiver. In particular, we assume that the only information that the receiver has access to is the observation vector \mathbf{y} , the signal constellation \mathcal{X} , and (possibly) the structure of the underlying channel model.²

Our goal is to design a low-complexity blind channel equalizer, so that reliable reconstruction of the transmitted symbols \mathbf{x} can be performed from the equalizer output $\tilde{\mathbf{x}}$ via a (possibly) low-complexity demapper.

III. PRELIMINARIES

In this section, we start with a brief introduction to variational inference and the VAE framework. We then describe the VAE-based blind channel equalizer, followed by a brief discussion of its limitations.

A. Variational Inference and Variational Autoencoder

In variational inference, the posterior distribution $p(\mathbf{x}|\mathbf{y})$ over a set of latent variables \mathbf{x} given some observed data \mathbf{y} is approximated by a variational distribution $q_\phi(\mathbf{x}|\mathbf{y}) \in \mathcal{Q}$, where \mathcal{Q} is a family of densities over \mathbf{x} , characterized by a set of free variational parameters ϕ .³ The goal of variational inference is to find the set of parameters ϕ such that the variational

approximation $q_\phi(\mathbf{x}|\mathbf{y})$ is closest to the true posterior $p(\mathbf{x}|\mathbf{y})$ in terms of the Kullback-Leibler (KL) divergence [31], i.e.,

$$q_\phi(\mathbf{x}|\mathbf{y}) = \arg \min_{q_\phi(\mathbf{x}|\mathbf{y}) \in \mathcal{Q}} \text{D}_{\text{KL}}(q_\phi(\mathbf{x}|\mathbf{y})||p(\mathbf{x}|\mathbf{y})). \quad (2)$$

Hence, finding the posterior distribution is cast as an optimization problem for which the complexity of the optimization is determined by the complexity of the density family \mathcal{Q} .

Since the true posterior $p(\mathbf{x}|\mathbf{y})$ is unknown, the KL divergence $\text{D}_{\text{KL}}(q_\phi(\mathbf{x}|\mathbf{y})||p(\mathbf{x}|\mathbf{y}))$ cannot be evaluated directly, thus hindering the optimization of $q_\phi(\mathbf{x}|\mathbf{y})$. However, the KL divergence can be rewritten as

$$\begin{aligned} \text{D}_{\text{KL}}(q_\phi(\mathbf{x}|\mathbf{y})||p(\mathbf{x}|\mathbf{y})) \\ = \text{D}_{\text{KL}}(q_\phi(\mathbf{x}|\mathbf{y})||p(\mathbf{x})) - \mathbb{E}_{q_\phi(\mathbf{x}|\mathbf{y})} \{\ln(p(\mathbf{y}|\mathbf{x}))\} + \ln(p(\mathbf{y})), \end{aligned} \quad (3)$$

where $\ln(p(\mathbf{y}))$ is independent of $q_\phi(\mathbf{x}|\mathbf{y})$. Hence, minimizing the KL divergence is equivalent to maximizing the ELBO defined as

$$\text{ELBO}(\phi) = \mathbb{E}_{q_\phi(\mathbf{x}|\mathbf{y})} \{\ln(p(\mathbf{y}|\mathbf{x}))\} - \text{D}_{\text{KL}}(q_\phi(\mathbf{x}|\mathbf{y})||p(\mathbf{x})), \quad (4)$$

for which the maximum is achieved when $q_\phi(\mathbf{x}|\mathbf{y}) = p(\mathbf{x}|\mathbf{y})$.

Maximizing the ELBO requires evaluating the expectation of the log-likelihood $\ln(p(\mathbf{y}|\mathbf{x}))$. In many practical applications, the likelihood $p(\mathbf{y}|\mathbf{x})$ is unknown or is difficult to obtain, thus making the direct maximization of the ELBO challenging. A promising solution for this problem has been proposed using the VAE framework, in which an additional parametric function $p_\theta(\mathbf{y}|\mathbf{x}) \in \mathcal{P}$, where \mathcal{P} is a family of densities, is introduced to approximate the true likelihood $p(\mathbf{y}|\mathbf{x})$. Then, the parameter sets $\boldsymbol{\theta}$ and ϕ that characterize the approximated posterior $q_\phi(\mathbf{x}|\mathbf{y})$ and approximated likelihood $p_\theta(\mathbf{y}|\mathbf{x})$ can be optimized simultaneously by searching over all possible combinations of ϕ and $\boldsymbol{\theta}$ that maximize the approximation of the ELBO,

$$(\boldsymbol{\theta}, \phi) = \arg \max_{\boldsymbol{\theta} \in \Theta, \phi \in \Phi} \text{ELBO}(\boldsymbol{\theta}, \phi), \quad (5)$$

where

$$\text{ELBO}(\boldsymbol{\theta}, \phi) = \mathbb{E}_{q_\phi(\mathbf{x}|\mathbf{y})} \{\ln(p_\theta(\mathbf{y}|\mathbf{x}))\} - \text{D}_{\text{KL}}(q_\phi(\mathbf{x}|\mathbf{y})||p(\mathbf{x})), \quad (6)$$

and Φ and Θ are the search space of ϕ and $\boldsymbol{\theta}$, respectively. In the machine learning literature, $q_\phi(\mathbf{x}|\mathbf{y})$ is often referred to as the inference/recognition model and $p_\theta(\mathbf{y}|\mathbf{x})$ as the corresponding generative model. However, in the communication setup, we find it more intuitive to use a different terminology: we refer to $p_\theta(\mathbf{y}|\mathbf{x})$ as the *encoder* and to $q_\phi(\mathbf{x}|\mathbf{y})$ as the corresponding *decoder*.⁴ Typically, $q_\phi(\mathbf{x}|\mathbf{y})$ and $p_\theta(\mathbf{y}|\mathbf{x})$ are implemented as NNs, where ϕ and $\boldsymbol{\theta}$ are the corresponding NN parameters [32]. However, it should be noted that in case a suitable model, e.g., the encoder $p_\theta(\mathbf{y}|\mathbf{x})$ is available, one can use this model instead of an NN, as it is done in [27].

²For the nonlinear channel case presented in Section VI, the receiver does not know the exact channel model. Instead, we assume the channel can be modeled by an NN.

³Note that a realization of \mathbf{y} is generated according to $p(\mathbf{y}|\mathbf{x})$ (i.e., the true channel) given some latent variables \mathbf{x} (i.e., the transmitted symbols).

⁴The same terminology was used in [27]. In the machine learning literature, $q_\phi(\mathbf{x}|\mathbf{y})$ is often referred to as the encoder while $p_\theta(\mathbf{y}|\mathbf{x})$ is the corresponding decoder.

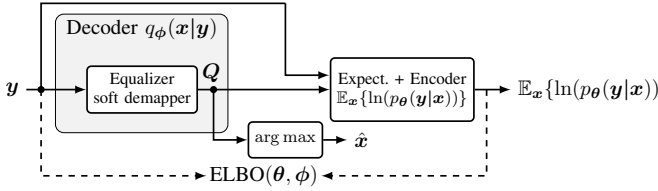


Fig. 2. Blind channel equalization and estimation using VAE, where the expectation in the expectation/encoder block is evaluated w.r.t. $\mathbf{x} \sim q_\phi(\mathbf{x}|\mathbf{y})$. The arg max block generates a hard decision of the transmitted message \hat{x}_k according to $\hat{x}_k = \mathcal{X}_{\hat{m}_k}$, where $\hat{m}_k = \arg \max_m (Q_k)_m$, and is only used during SER evaluation.

B. Blind Channel Equalization Using VAEs

Blind channel equalization (and demapping) using VAEs was originally proposed in [25]. The basic idea is to reinterpret channel equalization (and demapping) as a *variational inference* problem, for which the goal is to find a parametric function (i.e., a variational approximation) that faithfully approximates the MAP detector [25]–[27]. To do so, as depicted in Fig. 2, the approach uses a VAE decoder $q_\phi(\mathbf{x}|\mathbf{y}) : \mathbb{C}^{KN \times 1} \rightarrow \mathbb{R}^{N \times M}$ to generate soft estimates $\mathbf{Q} \in \mathbb{R}^{N \times M}$ of the transmitted symbols \mathbf{x} from the channel observation \mathbf{y} , and a corresponding VAE encoder $p_\theta(\mathbf{y}|\mathbf{x}) : \mathbb{C}^{(K+1)N \times 1} \rightarrow \mathbb{R}$ to generate the conditional probability distribution of receiving \mathbf{y} given $\mathbf{x} \sim q_\phi(\mathbf{x}|\mathbf{y})$ is transmitted. During the VAE training, the expectation of the log-likelihood, $\mathbb{E}_{q_\phi(\mathbf{x}|\mathbf{y})} \{\ln(p_\theta(\mathbf{y}|\mathbf{x}))\}$, is evaluated. Here, it is assumed that the transmitted symbols \mathbf{x} are independently modulated and the inter-symbol interference (ISI) caused by the channel has been mitigated. Therefore, it holds that $q_\phi(\mathbf{x}|\mathbf{y}) = \prod_{k=1}^N q_\phi(x_k|\mathbf{y})$, and we define $Q_{k,m} \triangleq q_\phi(x_k = \mathcal{X}_m|\mathbf{y})$. The VAE approach jointly optimizes the parameters of the VAE encoder and decoder by maximizing (5). Upon convergence, the VAE decoder can be viewed as an optimized equalizer.

Since $q_\phi(\mathbf{x}|\mathbf{y})$ generates soft demapping based on the channel observations, the VAE decoder also learns a soft demapper, which can be interpreted as an approximation of the MAP decoder. Furthermore, since the evidence $p(\mathbf{y}) = p(\mathbf{y}|\boldsymbol{\theta}^*)$ can be interpreted as the likelihood regarding the true channel parameters $\boldsymbol{\theta}^*$, the VAE encoder $p_\theta(\mathbf{y}|\mathbf{x})$ approximates the maximum-likelihood estimate of the channel [25]–[27]. This by-product can be used for applications such as localization [33], [34] and joint communication and sensing [35].

C. Limitations of the VAE-based Equalizer

Training of the VAE-based equalizer relies on maximizing the ELBO (6), which is commonly done by minimizing its opposite

$$\mathcal{L}(\boldsymbol{\theta}, \boldsymbol{\phi}) = -\text{ELBO}(\boldsymbol{\theta}, \boldsymbol{\phi}) \quad (7)$$

using (stochastic) gradient descent, where the trainable parameters $\boldsymbol{\lambda} = \{\boldsymbol{\theta}, \boldsymbol{\phi}\}$ are optimized according to $\boldsymbol{\lambda}_{t+1} = \boldsymbol{\lambda}_t - \eta \nabla_{\boldsymbol{\lambda}} \mathcal{L}(\boldsymbol{\lambda}_t)$, where η is the learning rate. Assuming a linear AWGN channel, the ELBO, thus (7), can

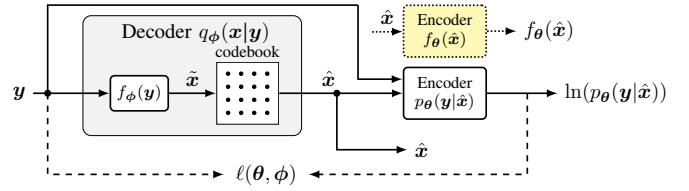


Fig. 3. Blind channel equalization and estimation using VQ-VAE. The inset (highlighted in yellow) indicates that the VQ-VAE encoder only outputs $f_\theta(\hat{\mathbf{x}})$ when $p_\theta(\mathbf{y}|\hat{\mathbf{x}}) \sim \mathcal{CN}(f_\theta(\hat{\mathbf{x}}), \sigma^2 \mathbf{I}_{KN})$ is assumed.

be evaluated numerically in closed-form (see [25]–[27] or Appendix A). It is then easy to compute the gradients with respect to the trainable parameters, thereby making VAE training straightforward (e.g. via gradient descent). However, for nonlinear channels that are modeled by nonlinear transfer functions, a closed-form expression for the ELBO is generally unavailable, making the VAE training challenging. In particular, to get the gradients of $\mathcal{L}(\boldsymbol{\theta}, \boldsymbol{\phi})$ with respect to the VAE decoder parameters $\boldsymbol{\phi}$, one needs to evaluate both $\nabla_{\boldsymbol{\phi}} \text{D}_{\text{KL}}(q_\phi(\mathbf{x}|\mathbf{y})||p(\mathbf{x}))$ and $\nabla_{\boldsymbol{\phi}} \mathbb{E}_{q_\phi(\mathbf{x}|\mathbf{y})} \{\ln(p_\theta(\mathbf{y}|\mathbf{x}))\}$. The former is easy to compute since $\text{D}_{\text{KL}}(q_\phi(\mathbf{x}|\mathbf{y})||p(\mathbf{x}))$ can often be evaluated analytically [25]. However, evaluating $\nabla_{\boldsymbol{\phi}} \mathbb{E}_{q_\phi(\mathbf{x}|\mathbf{y})} \{\ln(p_\theta(\mathbf{y}|\mathbf{x}))\}$ is more problematic due to the fact that (i) it is generally very challenging to obtain $\mathbb{E}_{q_\phi(\mathbf{x}|\mathbf{y})} \{\ln(p_\theta(\mathbf{y}|\mathbf{x}))\}$ in closed-form (e.g., when $p_\theta(\mathbf{y}|\mathbf{x})$ is implemented as an NN) and (ii) the Monte-Carlo approximation of $\mathbb{E}_{q_\phi(\mathbf{x}|\mathbf{y})} \{\ln(p_\theta(\mathbf{y}|\mathbf{x}))\}$ requires sampling from $q_\phi(\mathbf{x}|\mathbf{y})$, for which no proper gradients are defined with respect to $\boldsymbol{\phi}$ [32], thus preventing the VAE training via the gradient-based optimization methods. For continuous latent variables, an unbiased gradient approximation of $\nabla_{\boldsymbol{\phi}} \mathbb{E}_{q_\phi(\mathbf{x}|\mathbf{y})} \{\ln(p_\theta(\mathbf{y}|\mathbf{x}))\}$ can be obtained using the reparameterization trick [32]. However, for channel equalization, where the latent variables \mathbf{x} are discrete, the reparameterization trick cannot be applied.

Although gradient estimators such as Reinforce [36] or Markov-Chain-Monte-Carlo [37] exist in the literature, they are known to suffer from high variance or expensive computation and are therefore not considered in this paper.

IV. BLIND CHANNEL EQUALIZATION VQ-VAES

In this section, we first introduce the proposed framework for blind channel equalization using VQ-VAEs. We then introduce the associated loss function for the VQ-VAE-based equalizer training.

A. Blind Channel Equalization Using VQ-VAEs

Figure 3 visualizes the proposed VQ-VAE-based channel equalizer (and estimator). In addition to the encoder and the corresponding decoder of a conventional VAE-based equalizer (see Section III-B), the proposed scheme also requires a discrete codebook component. In the machine learning literature, when the VQ-VAE is used as a generative model, the codebook is typically unknown and is jointly trained with the encoder/decoder from data. However, in a communication

system where the latent variables (i.e., the transmitted symbols) are sampled from a known distribution, we use a fixed codebook, which is the same as the constellation set \mathcal{X} . Similar to the conventional VAE-based method, the VQ-VAE decoder acts as the channel equalizer and demapper, while its corresponding VQ-VAE encoder can be interpreted as the channel estimator.⁵ However, it should be highlighted that in contrast to the conventional VAE-based method, where the VAE decoder jointly learns channel equalization and soft demapping, our proposed VQ-VAE decoder learns the channel equalizer $f_\phi(\mathbf{y}) : \mathbb{C}^{KN \times 1} \rightarrow \mathbb{C}^{N \times 1}$ only, while symbol demapping is performed by a following pre-defined hard demapper. In particular, the channel equalizer takes the channel observation \mathbf{y} as input and outputs a vector of equalized symbols $\tilde{\mathbf{x}} = f_\phi(\mathbf{y})$. Then, the decoded symbol vector $\hat{\mathbf{x}} \in \mathcal{X}^N$ is obtained as

$$\hat{\mathbf{x}} = \arg \min_{\mathbf{x} \in \mathcal{X}^N} \|\tilde{\mathbf{x}} - \mathbf{x}\|^2, \quad (8)$$

where, similar to the conventional VAE-based approach, it is assumed that the equalized signals are mutually independent i.e., the transmitted symbols are independently modulated and the ISI caused by the channel memory has been mitigated by the equalizer. Note that (8) can be implemented with low-complexity as each equalized symbol \tilde{x}_k can be demapped individually according to

$$\hat{x}_k = \arg \min_{x \in \mathcal{X}} |\tilde{x}_k - x|^2. \quad (9)$$

Since the demapper considers hard demapping and is independent of the decoder parameters ϕ , we can express the joint transfer function $q_\phi(\mathbf{x}|\mathbf{y})$ of the equalizer and the demapper as

$$q_\phi(\hat{\mathbf{x}}|\mathbf{y}) = \begin{cases} 1 & \hat{\mathbf{x}} = \arg \min_{\mathbf{x} \in \mathcal{X}^N} \|\tilde{\mathbf{x}} - \mathbf{x}\|^2 \\ 0 & \text{otherwise,} \end{cases} \quad (10)$$

which can be interpreted as a one-hot categorical distribution, and is used as the variational approximation of the MAP decoder. In fact, (9) is essentially the widely used minimum Euclidean distance demapper, which has low complexity and is optimal for the AWGN channel. As for the VQ-VAE encoder $p_\theta(\mathbf{y}|\hat{\mathbf{x}}) : \mathbb{C}^{(K+1)N \times 1} \rightarrow \mathbb{R}$, it generates the conditional probability distribution $p_\theta(\mathbf{y}|\hat{\mathbf{x}})$ of observing \mathbf{y} given $\hat{\mathbf{x}}$ is transmitted.

B. VQ-VAE-based Equalizer Training

To train the proposed VQ-VAE-based channel equalizer and estimator, we use the following loss function

$$\ell(\phi, \theta) = -\mathbb{E}_{q_\phi(\mathbf{x}|\mathbf{y})} \{\ln(p_\theta(\mathbf{y}|\mathbf{x}))\} + \rho \|\tilde{\mathbf{x}} - \hat{\mathbf{x}}\|^2 \quad (11)$$

$$= -\ln(p_\theta(\mathbf{y}|\hat{\mathbf{x}})) + \rho \|\tilde{\mathbf{x}} - \hat{\mathbf{x}}\|^2, \quad (12)$$

which is similar to [28, eq. (3)] but without the term corresponding to the codebook training. Here, (12) is obtained

⁵Note that a different terminology is used in [28], where only $f_\phi(\mathbf{y})$ (i.e., our equalizer) is referred to as the VQ-VAE encoder and $p_\theta(\mathbf{y}|\hat{\mathbf{x}})$ is the corresponding decoder. However, we keep our terminology consistent with the VAE-based approach [27], and we find this definition more intuitive from a communication point of view.

TABLE I
VAE PARAMETERS: (I) AWGN CHANNEL WITH LINEAR DISPERSION, (II) OPTICAL FIBER CHANNEL, AND (III) AWGN CHANNEL PA NONLINEARITY

	VQ-VAE encoder $p_\theta(\mathbf{y} \mathbf{x})$			VQ-VAE decoder $q_\phi(\mathbf{x} \mathbf{y})$			
	layer	input	hidden	output	input	hidden	output
(i)	# of layers # of neurons act. function	- 25 × 2 -	- - -	- 2 linear	- 31 × 2 -	- - -	- 2 linear
(ii)	# of layers # of neurons act. function	- 62 -	2 64/32/5 ReLU	- 2 linear	- 127 × 2 -	3 32/8 ReLU	- 2 linear
(iii)	# of layers # of neurons act. function	- 46 -	3 64/32 ReLU	- 2 linear	- 95 × 2 -	3 64/16 ReLU	- 2 linear

×2: We use real-valued NN, and each complex number is represented by 2 neurons. For the linear channel, the VQ-VAE is implemented as finite impulse response (FIR) filters, and therefore there are no hidden layers.

by substituting (10) into (11), the dependence of (12) on ϕ is implicit through $\hat{\mathbf{x}}$, and $\rho > 0$ is a hyperparameter that can be optimized to improve the convergence behavior of the VQ-VAE training. The first term on the right-hand side of (12) is the reconstruction loss similar to the one in (6), but with the difference that the expectation of the log-likelihood with respect to the approximated posterior in (11) disappears due to (10). As a result, the cumbersome requirement of computing $\nabla_\phi \mathbb{E}_{q_\phi(\mathbf{x}|\mathbf{y})} \{\ln(p_\theta(\mathbf{y}|\mathbf{x}))\}$ for the conventional VAE-based equalizer training is circumvented. We highlight that even in the case where $\nabla_\phi \mathbb{E}_{q_\phi(\mathbf{x}|\mathbf{y})} \{\ln(p_\theta(\mathbf{y}|\mathbf{x}))\}$ for the conventional VAE-based approach can be solved analytically, our proposed method has (i) lower computational complexity as it does not require evaluating the expectation of the log-likelihood, and (ii) better performance as we shall see in the result sections. However, it should be noted that no gradient is defined for (8). We approximate the gradient of the decoder using the straight-through estimator [38] by copying the gradients from the encoder input $\hat{\mathbf{x}}$ to the decoder output $\tilde{\mathbf{x}}$. As for the second term in (12), which we refer to as the commitment loss, it drags the equalizer output to stay close to the codebook. In fact, one may find it similar to the training objective used for a DD-LMS equalizer with a batch-wise updating scheme. However, it should be noted that the DD-LMS equalizer requires using training overhead or the CMA for pre-convergence, which is not the case for the proposed method.

In practice, depending on the type of data that one wants to model, it is common to assume $p_\theta(\mathbf{y}|\mathbf{x})$ to be Bernoulli or Gaussian distributed [32]. In the communication setup, we follow the latter assumption as the noise in communication channels is commonly assumed to be Gaussian distributed. In particular, we assume $p_\theta(\mathbf{y}|\hat{\mathbf{x}}) \sim \mathcal{CN}(f_\theta(\hat{\mathbf{x}}), \sigma^2 \mathbf{I}_{KN})$, where $f_\theta(\hat{\mathbf{x}})$ and σ^2 are generated by the VQ-VAE encoder. It then holds that minimizing (12) is equivalent to minimizing [39]

$$\ell(\theta, \phi) = \|\mathbf{y} - f_\theta(\hat{\mathbf{x}})\|^2 + \rho \|\tilde{\mathbf{x}} - \hat{\mathbf{x}}\|^2, \quad (13)$$

since the minimum of the negative log-likelihood of a Gaussian distribution $p_\theta(\mathbf{y}|\hat{\mathbf{x}}) \sim \mathcal{CN}(f_\theta(\hat{\mathbf{x}}), \sigma^2 \mathbf{I}_{KN})$ is always

achieved at $\mathbf{y} = f_\theta(\hat{\mathbf{x}})$.⁶ In the remainder of this paper, our VQ-VAE encoder (shown in the inset of Fig. 3) generates $f_\theta(\hat{\mathbf{x}})$ only and is trained using (13) (or its variants presented in Section VI-A2).

V. RESULTS: LINEAR CHANNEL

In this section, we evaluate the proposed equalizer over an AWGN channel with memory described by $\mathbf{y} = \mathbf{h} * \mathbf{x} + \mathbf{n}$, where \mathbf{h} is the channel impulse response, $*$ denotes the convolution operator, and $\mathbf{n} \sim \mathcal{CN}(\mathbf{0}, \sigma_w^2 \mathbf{I}_N)$ is independent and identically distributed (i.i.d.) Gaussian noise, where σ_w^2 is the noise variance. For the scenarios considered in this paper, all equalizers (except for the CMA) are implemented in Python with the PyTorch framework, and training is performed by minimizing their corresponding cost functions using the Adam optimizer [40]. As for the CMA, it is trained according to its standard implementation with one equalizer update for each processed symbol and a learning rate scheduling scheme similar to [27].

A. Setup

The considered communication setup is depicted in Fig. 1, where the transmitted symbols are i.i.d. M -QAM symbols, the upsampling rate is $R = 2$, and the root-raised-cosine (RRC) filter with 10% roll-off is used as the PS filter. As in [25]–[27], the communication channel under consideration is a linear AWGN channel with

$$\mathbf{h} = (0.055 + j0.05, 0.283 - j0.120, -0.768 + j0.279, -0.064 - j0.058, 0.047 - j0.023),$$

where the noise variance of the AWGN is chosen from a range of considered signal-to-noise ratios (SNRs), which we define as $\mathbb{E}\{|x_k|^2\}/\sigma_w^2$. Since $R = 2$ is used as the upsampling rate and we consider operating the proposed equalizer on 2 SPS, no resampling is performed prior to channel equalization.

1) *VQ-VAE realization and training*: Similar to [27], we implement both the VQ-VAE encoder and decoder as linear FIR filters with Dirac initialization. However, we highlight again that in contrast to [27], our proposed equalizer does not require a soft demapping block at the training stage and therefore has lower computational complexity.⁷ We note that one can also implement the channel equalizer as an NN (see [25]–[27]). However, the NN-based equalizer in general requires more trainable parameters but does not bring performance improvement for the linear channel case [27, Fig. 7], and is therefore not considered here. The detailed VQ-VAE configurations are summarized in Table I, and we train our proposed VQ-VAE by minimizing (14) with $\rho = 1$ using stochastic gradient descent; in Section V-B3, we study the impact of ρ on the VQ-VAE training. The training dataset

⁶Note that ρ in (13) is different from the one in (12), where the former one is scaled by σ^{-2} . The effect of σ^{-2} in (13) is absorbed in ρ , which is a hyperparameter that we optimize for the VQ-VAE training.

⁷In case a soft demapping block is required to cope with the soft-decision forward error correction (FEC), a standard Gaussian demapper can be used once the equalizer has converged.

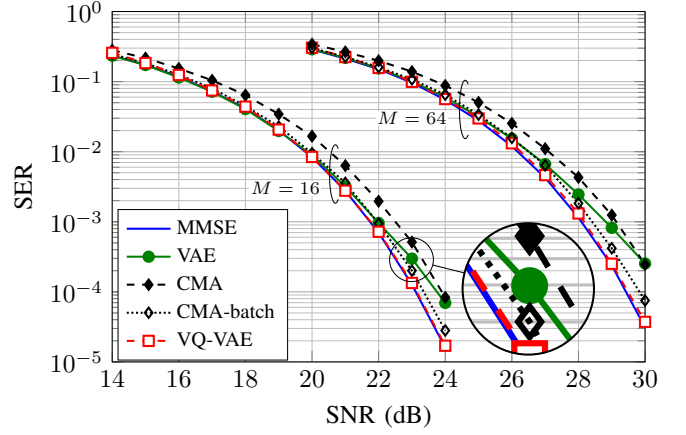


Fig. 4. SER performance over a linear AWGN channel with finite memory, a separate equalizer is trained for each data point shown in the figure.

contains 2^{16} symbols, the batch size is $N = 1024$ (corresponding to 2048 samples), and the learning rate is $\eta = 0.001$. The reference equalizers (except the CMA) are trained with the same batch size (i.e., $N = 1024$). However, for each reference equalizer, the learning rate is optimized within the set $\{1, 2, 5, 0.1, 0.2, 0.5, 0.01, 0.02, 0.05\} \times 10^{-2}$, i.e., we use the η that achieves the best performance.

B. Results and Discussions

1) *SER versus SNR*: The symbol error rate (SER) achieved by the proposed VQ-VAE is shown in Fig. 4, where a separate equalizer is trained for each data point. For comparison, we also show the SER achieved by the conventional VAE-based and the CMA-based channel equalizer. The CMA is phase insensitive and an additional phase recovery block is required prior to symbol detection. In this paper, we consider a genie-aided phase recovery, so that no performance penalty is introduced in the phase-recovery block. Moreover, we provide the performance that can be achieved by a data aided feed-forward equalizer (FFE), for which the mean squared error is chosen as the training criterion. Upon convergence, the data aided FFE resembles the MMSE equalizer, and we therefore do not distinguish these two equalizers in the following. For both 16-QAM and 64-QAM, the proposed method achieves the same performance as the data aided FFE, while outperforming the conventional VAE-based and the CMA-based equalizer, especially at high SNRs. One possible explanation for the performance gap between the conventional VAE and the VQ-VAE is that the soft demapping block in the conventional VAE requires the variance of the AWGN as input, which may lead to a mismatched decoding criterion in case where residual ISI remains or the estimated noise variance does not represent the real one sufficiently well.⁸

In order to close the performance gap between the CMA and the proposed equalizer, we implement a blind equalizer using

⁸One possible solution for mitigating the performance loss due to the mismatched soft demapping can be found in [41], where the authors propose to obtain the noise variance from the mutual information estimate.

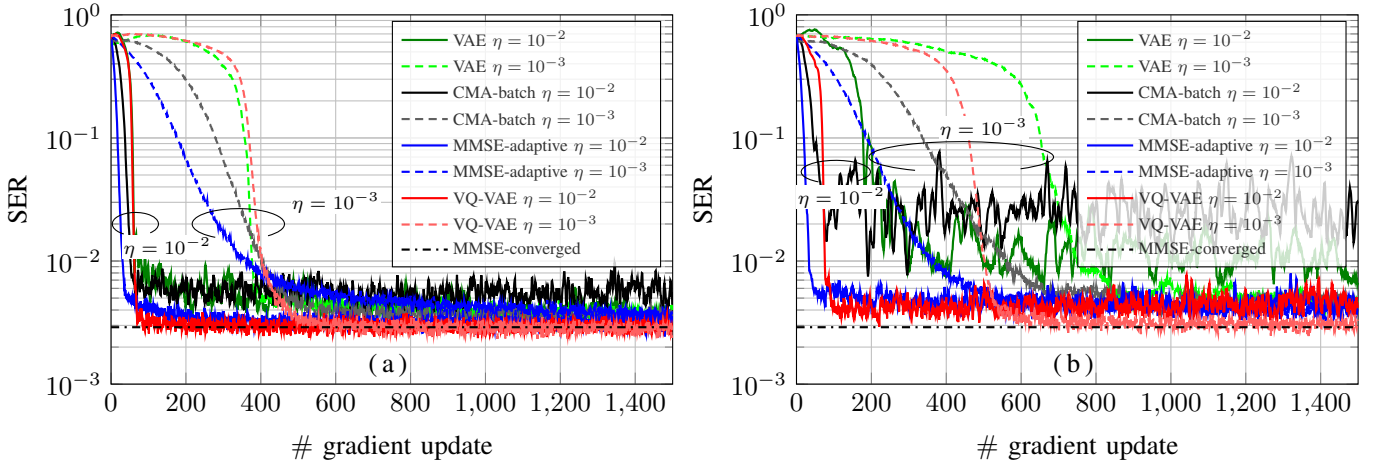


Fig. 5. Convergence behavior of four channel equalizers for 16-QAM transmission at SNR = 21 dB: (a) each gradient update utilizes $N = 1024$ symbols; (b) each gradient update utilizes $N = 64$ symbols.

a batch-wise updating scheme, for which the constant modulus criterion is used as the cost function for training.⁹ The SER of the resulting equalizer, which we denote by CMA-batch, is also shown in Fig. 4. It can be seen that the CMA-batch outperforms the standard CMA and the conventional VAE (at high SNRs), but does not perform as well as the data aided FFE or the proposed VQ-VAE-based approach. We attribute the remaining performance gap between CMA-batch and the data aided FFE to the fact that the constant modulus criterion is ill-conditioned for high-order modulation formats.

2) *Convergence behavior*: We now study the convergence behavior of our proposed method and compare it with the reference schemes. For all equalizers under investigation, we consider 16-QAM transmission at SNR = 21 dB with training data generated on the fly (i.e., new training data is generated after each gradient update). Figure 5 shows the SER evolution of different equalizers as we increase the number of performed gradient updates. The number of symbols used for each gradient update is $N = 1024$ for Fig. 5(a) and $N = 64$ for Fig. 5(b). For the considered configurations, we observe that: (i) A large batch size in general leads to better convergence behavior for all studied equalizers, which is expected as a larger batch size results in a smaller variance in the gradient estimate. However, it should be noted that a large batch size is more computationally demanding and requires slower variations in the channel. There exists an “optimal” value that trades off the performance against the computational complexity and convergence speed. (ii) The proposed VQ-VAE-based approach is more robust to variations in batch size and learning rate. In particular, for different batch sizes and learning rates under investigation, the proposed method always achieves the best SER performance among all considered equalizers upon convergence, which we believe to be advantageous for time-varying channels. (iii) For a large batch size $N = 1024$, a large learning rate generally leads to faster convergence for all considered equalizers, except that the CMA-batch suffers from training instability. The proposed equalizer has very

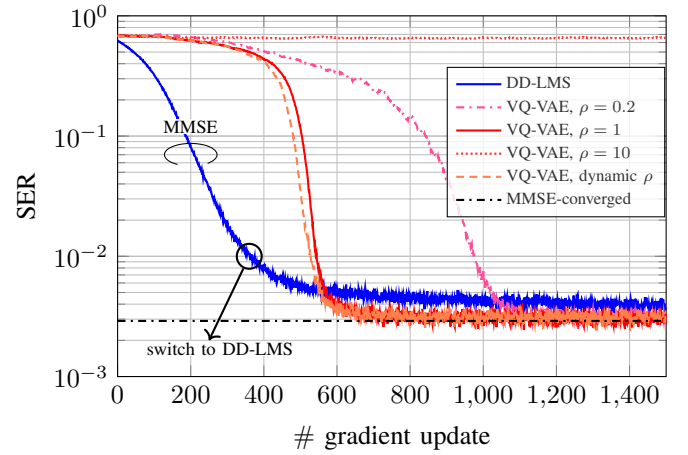


Fig. 6. Convergence behavior of the VQ-VAE-based and DD-LMS equalizer for 16-QAM transmission at SNR = 21 dB. The learning rate is $\eta = 10^{-2}$ and the number of symbols used for each gradient update is $N = 64$ for both the VQ-VAE-based and DD-LMS equalizer.

similar convergence behavior as the conventional VAE, while having a slightly slower starting convergence rate than the CMA-batch and the data aided FFE. However, it should be highlighted that among all considered equalizers, the proposed approach requires fewest gradient updates to converge to the “optimal” performance. (iv) For a small batch size $N = 64$, the proposed equalizer is able to converge to the “optimal” performance, while all reference equalizers exhibit a certain level of SER penalty, especially for a relatively large learning rate $\eta = 10^{-2}$.

3) *Impact of ρ and comparison with DD-LMS*: We now study the impact of the hyperparameter ρ on the VQ-VAE training. Figure 6 visualizes the SER as a function of the number of gradient updates. It is shown that for $\rho = 0.2$, the VQ-VAE-based channel equalizer requires more gradient updates to converge as compared to $\rho = 1$. However, for $\rho = 10$, the VQ-VAE-based equalizer fails to converge. Such a behavior is expected due to the fact that when ρ is set to a large value, the proposed equalizer resembles a DD-LMS equalizer

⁹Although the standard CMA implementation updates the filter taps for each processed symbol, it is also common to use batch-wise updating scheme to enable parallelized data processing (see e.g., [42], [43]).

TABLE II
FIBER PARAMETERS

SSMF			NZDSF		
α (dB/km)	β (ps ² /km)	γ (W · km) ⁻¹	α (dB/km)	β (ps ² /km)	γ (W · km) ⁻¹
0.2	-21.683	1.3	0.21	-4.0	1.6

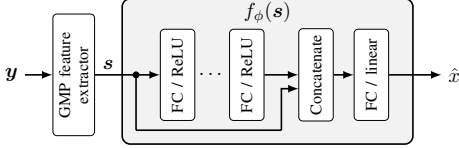


Fig. 7. Structure of the NN-based channel equalizer employing fully connected architecture and a residual connection that connects the NN input directly to the output layer. The feature extractor block generates the nonlinear feature vector as described in Section VI-A2.

with batch-wise updating scheme, and will inevitably suffer from convergence issues if no proper pre-training is performed. To avoid the need for optimizing ρ manually, we modify (13) to the loss function

$$\ell(\phi, \theta) = \psi_t \|\mathbf{y} - f_\theta(\hat{\mathbf{x}})\|^2 + (1 - \psi_t) \|\tilde{\mathbf{x}} - \hat{\mathbf{x}}\|^2, \quad (14)$$

where $t > 0$ is the iteration index and

$$\psi_{t+1} = \frac{\|\mathbf{y} - f_\theta(\hat{\mathbf{x}})\|^2}{\|\mathbf{y} - f_\theta(\hat{\mathbf{x}})\|^2 + \|\tilde{\mathbf{x}} - \hat{\mathbf{x}}\|^2} \Big|_t, \quad (15)$$

with $\psi_0 = 0.5$ and $f(\cdot)|_t$ indicates evaluating $f(\cdot)$ at t -th iteration. This new loss function dynamically balances the importance of the reconstruction error and the commitment loss. The learning curve obtained using (15) is shown in Fig. 6. Last but not least, we show the learning curve of a DD-LMS equalizer, for which the equalizer taps are pre-conditioned in a data aided manner using the MMSE criterion. Once the SER reaches 10^{-2} , we switch the equalizer to the decision-directed mode. The resulting SER evolution is shown in Fig. 6, where it is shown that the DD-LMS equalizer does not perform as well as the proposed VQ-VAE-based equalizer.

VI. RESULTS: NONLINEAR CHANNELS

To validate the effectiveness of the proposed method for nonlinear channels, we evaluate our proposed equalizer over two nonlinear scenarios namely (i) transmission over an unamplified optical fiber channel and (ii) transmission over a wireless channel with nonlinear PA. Since both fiber and PA nonlinearity are highly dependent on the transmit power, for all results presented in the following, a separate equalizer is trained for each power level.

A. Nonlinear Optical Fiber Channel

We start with evaluating the performance of the proposed method over an unamplified optical fiber link, for which typical use cases include data center interconnects with a range of 80 – 120 km. To support transmission over 80 km and beyond, such systems are required to operate at a (relatively) high launch power and often exhibit moderate/high fiber nonlinearity.

1) *Setup*: The considered system transmits a single channel waveform of 25 GBaud over a single span fiber link of 110 km. The PS filter is the RRC filter with 10% roll-off and the oversampling rate is set to $R = 8$ to ensure that the spectral broadening effect due to fiber nonlinearity is fully captured in the simulation. To cover different scenarios, we consider two test cases with different level of fiber nonlinearity: (i) transmission over the standard single mode fiber (SSMF) and (ii) transmission over the non-zero dispersion-shifted fiber (NZDSF). The optical signal propagation along the fiber is simulated by solving the nonlinear Schrödinger equation via the split-step Fourier method (SSFM) with 100 steps.¹⁰ The fiber parameters used in the simulation are summarized in Table II. At the receiver, AWGN is added to the fiber output to emulate the shot noise from the coherent receiver. Similar to [44], we consider a coherent receiver with a minimum sensitivity of -20 dBm, and the amount of noise that is added to the fiber output signal is -33.5 dBm. In a back-to-back setup, such a configuration will allow for achieving a pre-FEC bit error rate (BER) of $1.25 \cdot 10^{-2}$, which is the maximum BER that can be tolerated by the FEC block in the 400ZR standard [45] to fulfill the post decoding error rate requirements. The resulting waveform is then low-pass filtered by a brick-wall filter with 45 GHz bandwidth and sampled at a sampling rate of 50 GHz (i.e., to have 2 SPS), after which a static filter is applied to perform a coarse (i.e., 90% in our simulations) dispersion compensation.¹¹ Finally, channel equalization is performed prior to symbol detection.

2) *VQ-VAE realization and training*: Traditional methods using linear FIR filters cannot model or equalize the nonlinear optical fiber channel well. NNs on the other hand the ability to learn nonlinear and complex relationships in data. Therefore, we implement our VQ-VAE using a pair of NNs. In the literature, various NN architectures ranging from simple multi-layer perceptrons [6] to sophisticated models such as biLSTM [11] have been used for channel equalization. In this paper, we restrict ourselves to the fully-connected architecture due to its easy deployment and training. However, for the decoder NN (i.e., our channel equalizer), a residual connection that directly connects the input feature to the output layer is also employed as depicted in Fig. 7. Such a residual connection has been shown to improve the performance as well as NN training in several communication related applications [46]–[48]. Furthermore, instead of having the raw channel observations \mathbf{y} as input, our NN-based equalizer takes a nonlinear feature vector \mathbf{s}^k as input and generates the k -th equalized signal according to $\tilde{\mathbf{x}}_k = f_\phi(\mathbf{s}^k)$. Here, the nonlinear feature vector \mathbf{s}_k is constructed following the generalized memory polynomial (GMP) [49], which is a widely used model that relates the desired output (i.e., equalized signal $\tilde{\mathbf{x}}_k$) to the input

¹⁰No improvement of accuracy for the forward propagation was observed when further increasing the number of steps or the oversampling rate.

¹¹Here, we note that the dispersion compensation filter can in principle be integrated into the adaptive channel equalizer. However, the required equalizer length in such an implementation will increase linearly with the fiber length. In practice, it is more common to use a static filter to perform a coarse dispersion compensation prior to the adaptive filtering.

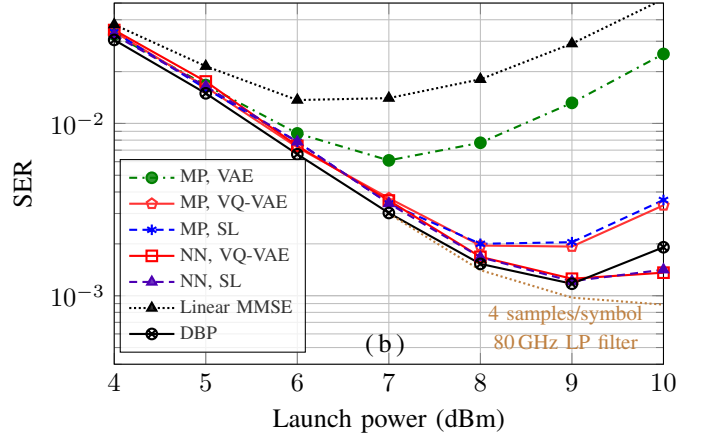
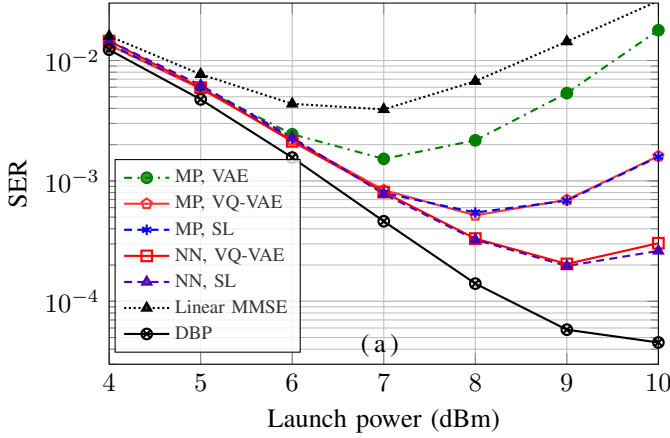


Fig. 8. SER as a function of launch power for transmission over an unamplified optical fiber link of 110 km: (a) standard single mode fiber with 90% dispersion pre-compensated; (b) non-zero dispersion-shifted fiber with 90% dispersion pre-compensated. Note that the DBP curve assumes performing the SSFM for 100 steps, which has very high complexity.

(i.e., observation \mathbf{y}) according to

$$\begin{aligned} \tilde{x}_k = & \sum_{p \in \mathcal{P}_a} \sum_{l \in \mathcal{L}_a^p} a_{p,l} \underbrace{y_{k-l} |y_{k-l}|^{p-1}}_{s_{p,l}^k} \\ & + \sum_{p \in \mathcal{P}_b} \sum_{l \in \mathcal{L}_b^p} \sum_{m \in \mathcal{M}_b} b_{p,l,m} \underbrace{y_{k-l} |y_{k-l-m}|^{p-1}}_{s_{p,l,m}^k} \\ & + \sum_{p \in \mathcal{P}_c} \sum_{l \in \mathcal{L}_c^p} \sum_{n \in \mathcal{M}_c} c_{p,l,m} \underbrace{y_{k-l} |y_{k-l+m}|^{p-1}}_{s_{p,l,n}^k}, \end{aligned} \quad (16)$$

where $a_{p,l}$, $b_{p,l,m}$, and $c_{p,l,m}$ are the model coefficients, \mathcal{P}_a , \mathcal{P}_b , and \mathcal{P}_c are the sets that contain the nonlinear orders, \mathcal{L}_a^p , \mathcal{L}_b^p , \mathcal{L}_c^p , \mathcal{M}_b , and \mathcal{M}_c are the sets that contain the memory taps. In our simulation, the nonlinear feature vector \mathbf{s}^k contains all $s_{p,l}^k$, $s_{p,l,m}^k$, and $s_{p,l,n}^k$ for $\mathcal{P}_a = \{1, 3, 5\}$, $\mathcal{P}_b = \mathcal{P}_c = \{3\}$, $\mathcal{L}_a^1 = \{-21, \dots, 21\}$, $\mathcal{L}_a^3 = \{-5, \dots, 5\}$, $\mathcal{L}_a^5 = \{-3, \dots, 3\}$, $\mathcal{L}_b = \mathcal{L}_c = \{5, \dots, 5\}$, and $\mathcal{M}_b = \mathcal{M}_c = \{1, 2, 3\}$. With this configuration, the constructed nonlinear features vector is of length 127. Our NN-based equalizer, summarized in Table I, is found to perform better than the one using a fully-connected architecture.¹²

The training of our proposed VQ-VAE is again performed by minimizing (13), but with slight modifications. In particular, we use L_2 regularization on the trainable weights in the input layer and the hidden layers of our equalizer NN. A similar regularization scheme has been previously used in [12], where it is shown that using a regularization term in the loss function can help to mitigate the so-called “jail window” effect observed in the equalized signal constellation when the regression loss is used for training [51]. Note that this jail window constellation can lead to a performance penalty unless it is handled properly [12], [51]. For optimization, our training dataset contains 65536 symbols, and the batch

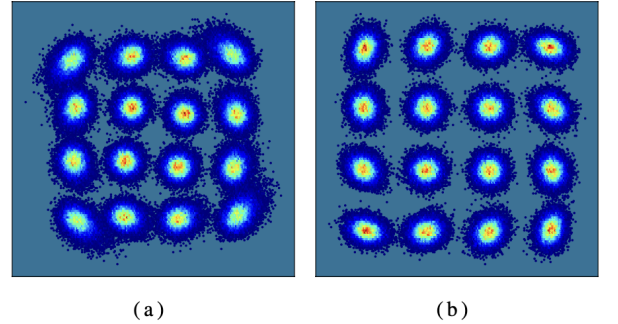


Fig. 9. Received signal constellations after channel equalization (a): Linear equalizer; (b) NN-based equalized trained with VQ-VAE. The symbol rate of the transmitted 16-QAM signal is 25 GBaud and the signal is propagated over the SSFM of 110km with a launch power of 8 dBm.

size and learning rate are set to $N = 2048$ and $\eta = 0.001$, respectively.

3) *SER versus launch power*: The SER (shown in red squares) achieved by the proposed VQ-VAE-based equalizer over a range of launch power is shown in Fig. 8(a) for the SSMF and in Fig. 8(b) for the NZDSF, respectively. For comparison, we also provide the SER achieved by an NN-based equalizer with the same NN configurations but trained using supervised learning (SL) (purple triangles), a data aided linear equalizer, and digital backpropagation (DBP) with 100 steps. It can be seen that for a low launch power (e.g., at 4 dBm), the performance gap between the linear equalizer and the nonlinear one is small, indicating that the SER is mostly dominated by the receiver noise. However, when increasing the launch power, the nonlinear distortion gets stronger, and the performance gap between the linear and nonlinear equalizer increases. In particular, the optimal transmit power for the linear equalizer is around 7 dBm, and is increased to around 9 dBm for the NN-based nonlinear equalizer. The increased optimal launch power indicates that systems employing the proposed nonlinear equalizer can support a longer transmission distance, which is essential for the unamplified optical fiber

¹²A similar approach has been applied in [14], [50], where nonlinear impairment features constructed from the first-order perturbation theory were used as the input to the NN-based equalizer. Also note that our configuration is only optimized for one launch power (i.e., 8 dBm). To further improve the SER performance or to reduce complexity, one may need to optimize the NN configuration (e.g., number of layers, NN architecture) for each launch power.

link.

In order to show the advantages of the proposed VQ-VAE-based equalizer over the VAE-based approach for the nonlinear channels, we derived a closed-form expression (see Appendix B) for the ELBO assuming that the nonlinear channel can be modeled by a memory polynomial (MP).¹³ When implementing both the encoder and decoder as MPs, the SER achieved by the MP-based VAE (green circles) and the MP-based VQ-VAE (red pentagons) is also shown in Fig. 8, where it can be seen that the proposed VQ-VAE-based equalizer significantly outperforms the VAE-based counterpart at high launch power.

Finally, it is noteworthy that the NN-based equalizer slightly outperforms DBP in the nonlinear regime for the NZDSF, although the optimal SER is essentially the same. A similar behavior was observed in [13], where it was justified that in the nonlinear regime, a significant part of the broadened spectrum of the received waveform is filtered out before processing. The missing spectrum is not properly backpropagated when using DBP, while the NN-based equalizer manages to somewhat compensate for that effect. Indeed, as we increase the bandwidth of the receiver and perform DBP with 4 SPS, the performance of DBP improves and is better than that of the NN-based equalizer.

Figure 9 visualizes the equalized signal obtained by using the linear FFE (left) and the proposed VQ-VAE-based equalizer with NN implementation (right) assuming transmission over the SSMF with a launch power of 8 dBm. Clearly, the signal constellation obtained using the NN-based equalizer is much less degraded compared to the one obtained using the linear FFE, albeit nonlinear distortion can still be observed even when the NN-based equalizer is applied. To further improve the performance of the NN-based equalizer, one may consider using different NN architectures such as the biLSTM [11] or the physics-informed one [13]. Here, we highlight that the proposed VQ-VAE-based equalizer is topology independent, and we do not focus on designing the optimal architecture of NN-based channel equalizers. Yet, we highlight that a hyperparameter optimization is performed in our simulation to find a low-complexity topology that achieves satisfying performance.

B. Nonlinear Wireless Channel with PA Nonlinearity

We now study a wireless scenario, where both linear and nonlinear distortion are introduced to the transmit signal by the non-ideal PA. We note that in the literature, it is customary to compensate for PA impairments at the transmitter side using digital pre-distortion (DPD) [52]. However, to optimize the DPD parameters, a feedback data acquisition path is typically required to collect the PA output signal [53]. To capture the full-band behavior of the PA, which is necessary for the DPD optimization, high sampling rate analog-to-digital converters are needed for the feedback path, which is challenging and expensive for wideband signals. Additionally, for

scenarios where low-cost and low-power consumption devices are preferred, e.g., the internet of things, transmitter-side DPD optimization may not be affordable. Therefore, we study the possibility of mitigating the transmitter-induced performance loss at the receiver-end using blind channel equalization.

1) *Setup*: The PA is modeled by a GMP, for which the nonlinear orders, the memory lengths, and the cross-term memory lengths are $\mathcal{P}_a = \mathcal{P}_b = \mathcal{P}_c = \{1, 2, 3, 4, 5, 6, 7\}$, $\mathcal{L}_a^p = \mathcal{L}_b^p = \mathcal{L}_c^p = \{0, 1, 2\}$ for all p , and $\mathcal{M}_b = \mathcal{M}_c = \{1\}$, respectively. The corresponding parameters of the GMP are estimated from the measurements of the RF WebLab,¹⁴ for which more detailed configurations can be found in [54]. Similar to [54], we consider the transmission of a 64-QAM signal over an AWGN channel, where the upsampling rate is $R = 2$, the PS filter is an RRC filter with 20% roll-off, and the AWGN has a fixed noise standard deviation $\sigma_{\text{ch}} = 0.4$ V. We vary the PA output power to emulate different operating SNRs.

2) *Equalizer realization and training*: Similar to the nonlinear fiber channel case, the proposed VQ-VAE is implemented as a pair of NNs, which have a very similar structure (but different hyper-parameters) as the ones used in Section VI-A. In particular, the equalizer NN also employs a residual connection (see Fig. 7) and the NN input s^k is constructed as described in Section VI-A2, where the model parameters are set to $\mathcal{P}_a = \{1, \dots, 7\}$, $\mathcal{P}_b = \mathcal{P}_c = \{3\}$, $\mathcal{L}_a^1 = \{-15, \dots, 15\}$, $\mathcal{L}_a^p = \{-3, \dots, 3\}$ for $p \neq 1$, $\mathcal{L}_b = \mathcal{L}_c = \{-3, \dots, 3\}$, and $\mathcal{M}_b = \mathcal{M}_c = \{1, 2, 3\}$. The NN parameters are summarized in Table I. As for training, we noticed that the nonlinear PA scenario requires using a larger batch size to achieve satisfying performance compared to the case of an unamplified optical fiber link. We attribute it to the fact that we now work with 64-QAM transmission and we operate at a lower SER. In our simulation, the training dataset contains 2^{18} symbols, the batch size is set to 2^{14} , and the learning rate is $\eta = 0.001$.

3) *SER versus averaged PA output power*: Figure 10 shows the achieved SER as a function of the average PA output power for the case of using a linear equalizer, the VQ-VAE-based equalizer (NN-based and MP-based), and the theoretical SER of 64-QAM over an AWGN. We observe that when the average PA output power is low, most of the input signal to the PA lies in the PA's linear region, and increasing the PA output power leads to improved SER performance (as the SNR is increased). As the average PA output power exceeds 33 dBm, the PA starts to operate in the medium-high nonlinear region, and the SER starts to increase when the receiver uses a linear equalizer. In the case where the proposed nonlinear equalizer is used, a substantial performance gain can be achieved compared to using a linear equalizer. In particular, the optimal average PA output power can be increased by around 1.5 dBm (from 33.5 dBm to 35 dBm), while the optimal SER is improved from $4 \cdot 10^{-4}$ to $5.5 \cdot 10^{-5}$.

To compare the proposed method with the customary implementation where the PA nonlinearity is compensated at the transmitter side, the SER achieved by a direct learning (DL)-

¹³Although a closed-form expression for the ELBO is available in this case, we note that the computational complexity of the VAE-based approach is much higher than the VQ-VAE-based method.

¹⁴The RF WebLab is a PA measurement setup that can be remotely accessed at www.dpdcompetition.com

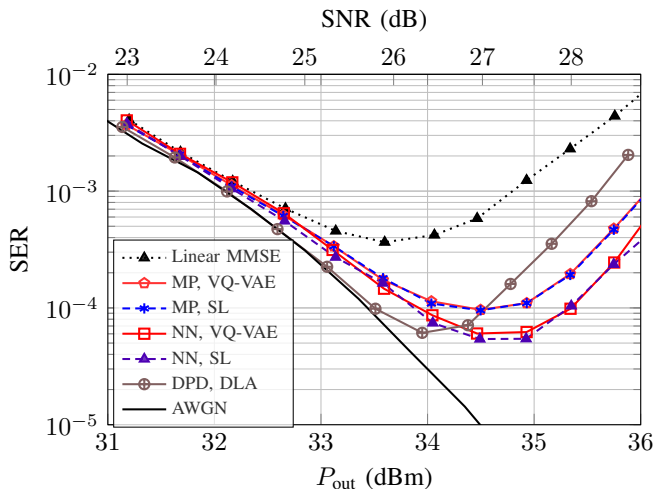


Fig. 10. SER performance in an AWGN channel where the transmitted signals are distorted by a nonlinear PA.

based DPD, implemented as an NN, is also provided [55]. It is shown that the proposed equalizer achieves essentially the same performance as a DL-based DPD in terms of SER. However, the DL-based DPD is shown to outperform the VQ-VAE-based equalizer at low launch power. We attribute the performance gap partially to the fact that the VQ-VAE-based equalizer is trained with data distorted by the AWGN, which is not the case for the DPD. As for high launch power (e.g., above 34 dBm), the proposed method significantly outperforms the DL-based DPD. We believe the performance gap comes from the fact that the input signal (after DPD) to the PA exhibits higher peaks and is therefore more distorted by the nonlinear PA.

VII. CONCLUSION

In this work, we proposed a novel approach to blind channel equalization using the VQ-VAE framework. We evaluate the performance of the proposed method over both a linear channel and two nonlinear scenarios including transmission over the unamplified optical fiber link and transmission over a wireless channel with PA nonlinearity. For the linear channel, the proposed method, where both the VQ-VAE encoder and decoder are implemented as linear FIR filters, is shown to achieve similar performance to a data aided equalizer using the MMSE criterion, while outperforming state-of-the-art blind equalizers including the CMA and VAE-based equalizers. Compared to the reference schemes, the proposed equalizer is also shown to exhibit better convergence behavior, which can be advantageous for time-varying channels. Moreover, contrary to the VAE-based approach that is designed for linear AWGN channels, we have shown that our proposed method can also converge for nonlinear channels, which is advantageous for many practical communication systems where nonlinear impairments are presented.

APPENDIX A CLOSED-FORM EXPRESSION FOR THE ELBO FOR A LINEAR AWGN CHANNEL

Consider the linear AWGN channel described by $\mathbf{y} = \mathbf{h} * \mathbf{x} + \mathbf{n}$, where \mathbf{h} is the channel impulse response, $*$ denotes the convolution operator, and $\mathbf{n} \sim \mathcal{CN}(\mathbf{0}, \sigma_w^2 \mathbf{I}_N)$ is i.i.d. Gaussian noise with variance σ_w^2 . The channel law (likelihood) $p_{\theta}(\mathbf{y}|\mathbf{x})$ follows the multivariate Gaussian distribution

$$p_{\theta}(\mathbf{y}|\mathbf{x}) = \frac{1}{(\pi\sigma_w^2)^N} e^{-\|\mathbf{y} - \mathbf{X}\mathbf{h}\|^2/\sigma_w^2}, \quad (17)$$

where $\theta = \{\mathbf{h}, \sigma_w^2\}$, $\mathbf{X}\mathbf{h} = \mathbf{h} * \mathbf{x}$, and

$$\mathbf{X} = (\mathbf{x}^{(L)}, \dots, \mathbf{x}^{(1)}, \mathbf{x}, \mathbf{x}^{(-1)}, \dots, \mathbf{x}^{(-L)}), \quad (18)$$

where $\mathbf{x}^{(l)} = (x_{1+l}, \dots, x_N, \mathbf{0}_l^{\top})^{\top}$, $\mathbf{0}_l$ denotes a length l column vector of all zero elements, and $\mathbf{x}^{(-l)} = (\mathbf{0}_l, x_1, \dots, x_{N-l})^{\top}$. It is assumed that the channel has $(2L+1)$ taps and y_k is related to $\{x_{k-L}, \dots, x_{k+L}\}$. Assuming the transmitted symbols are uniformly distributed (i.e., $p(\mathbf{x}) = M^{-N}$) and the outputs of the VAE equalizer are mutually independent (i.e., $q_{\phi}(x_i, x_j|\mathbf{y}) = q_{\phi}(x_i|\mathbf{y})q_{\phi}(x_j|\mathbf{y})$ for $i \neq j$), we have

$$\begin{aligned} \text{ELBO}(\phi, \theta) &= \mathbb{E}_{q_{\phi}(\mathbf{x}|\mathbf{y})} \{\ln(p(\mathbf{y}|\mathbf{x}))\} - \text{D}_{\text{KL}}(q_{\phi}(\mathbf{x}|\mathbf{y})\|p(\mathbf{x})) \\ &= -N \ln(\pi\sigma_w^2) - \frac{1}{\sigma_w^2} \mathbb{E}_{q_{\phi}(\mathbf{x}|\mathbf{y})} \{\|\mathbf{y} - \mathbf{X}\mathbf{h}\|^2\} \\ &\quad + \mathcal{H}(q_{\phi}(\mathbf{x}|\mathbf{y})) + N \ln(M) \\ &= -N \ln(\sigma_w^2) - \frac{1}{\sigma_w^2} A + \mathcal{H}(q_{\phi}(\mathbf{x}|\mathbf{y})) + C, \end{aligned} \quad (19)$$

where $\mathcal{H}(q_{\phi}(\mathbf{x}|\mathbf{y}))$ is the entropy of $q_{\phi}(\mathbf{x}|\mathbf{y})$, C is a constant independent of ϕ and θ , and

$$\begin{aligned} A &= \mathbb{E}_{q_{\phi}(\mathbf{x}|\mathbf{y})} \{\|\mathbf{y} - \mathbf{X}\mathbf{h}\|^2\} \\ &= \mathbf{y}^{\dagger} \mathbf{y} - 2\Re\{\mathbf{y}^{\dagger} \mathbb{E}_{q_{\phi}(\mathbf{x}|\mathbf{y})} \{\mathbf{X}\mathbf{h}\}\} + \mathbb{E}_{q_{\phi}(\mathbf{x}|\mathbf{y})} \{(\mathbf{X}\mathbf{h})^{\dagger} \mathbf{X}\mathbf{h}\} \\ &= \mathbf{y}^{\dagger} \mathbf{y} - 2\Re\{\mathbf{y}^{\dagger} \mathbb{E}_{q_{\phi}(\mathbf{x}|\mathbf{y})} \{\mathbf{X}\}\mathbf{h}\} + \mathbf{h}^{\dagger} \mathbb{E}_{q_{\phi}(\mathbf{x}|\mathbf{y})} \{\mathbf{X}^{\dagger} \mathbf{X}\}\mathbf{h}, \end{aligned}$$

where

$$\begin{aligned} &\mathbb{E}_{q_{\phi}(\mathbf{x}|\mathbf{y})} \{\mathbf{X}^{\dagger} \mathbf{X}\}_{i,j} \\ &= \begin{cases} \mathbb{E}_{q_{\phi}(\mathbf{x}|\mathbf{y})} \{\|\mathbf{x}^{(L-i)}\|^2\} & i = j \\ \mathbb{E}_{q_{\phi}(\mathbf{x}|\mathbf{y})} \{(\mathbf{x}^{(L-i)})^{\dagger}\} \mathbb{E}_{q_{\phi}(\mathbf{x}|\mathbf{y})} \{\mathbf{x}^{(L-j)}\} & i \neq j. \end{cases} \end{aligned}$$

APPENDIX B CLOSED-FORM EXPRESSION FOR THE ELBO FOR A NONLINEAR CHANNEL MODELED BY MP

Consider modeling the nonlinear channel using an MP [49] according to

$$y_k = \sum_{p \in \mathcal{P}} \sum_{l \in \mathcal{L}^p} c_{p,l} x_{k-l} |x_{k-l}|^p + n_k, \quad (20)$$

where \mathcal{P} and \mathcal{L}^p are the sets containing the nonlinear orders and memory lengths, x_k and y_k are the input and output to the channel at the k -th time step, $n_k \sim \mathcal{CN}(0, \sigma_w^2)$ is the AWGN, and $c_{m,k}$ denotes model coefficient, respectively. We can relate the channel output to the input in a compact matrix representation given by

$$\mathbf{y} = \mathbf{X}\mathbf{c} + \mathbf{n},$$

where $\mathbf{n} \sim \mathcal{CN}(\mathbf{0}, \sigma_w^2 \mathbf{I}_N)$ and

$$\mathbf{X}^\top = \begin{bmatrix} (\mathbf{x}^{(L)})^\top \\ \vdots \\ (\mathbf{x}^{(-L)})^\top \\ \vdots \\ (\mathbf{x}^{(L)}|\mathbf{x}^{(L)}|^{P})^\top \\ \vdots \\ (\mathbf{x}^{(-L)}|\mathbf{x}^{(-L)}|^{P})^\top \end{bmatrix}, \text{ and } \mathbf{c} = \begin{bmatrix} c_{0,L} \\ \vdots \\ c_{0,-L} \\ \vdots \\ c_{P,L} \\ \vdots \\ c_{P,-L} \end{bmatrix},$$

where, for notation convenience, it is assumed $\mathcal{L}^p = \{-L, \dots, L\}$ for all $p \in \mathcal{P} = \{1, \dots, P\}$. Then, the likelihood has the same form as (17), except that the convolution $\mathbf{h} * \mathbf{x}$ should be replaced by $\mathbf{X}\mathbf{c}$. Similarly, the ELBO can be evaluated in closed-form and is given by (19), but with

$$\begin{aligned} A &= \mathbb{E}_{q_\phi(\mathbf{x}|\mathbf{y})} \{ \|\mathbf{y} - \mathbf{X}\mathbf{h}\|^2 \} \\ &= \mathbf{y}^\dagger \mathbf{y} - 2\Re\{\mathbf{y}^\dagger \mathbb{E}_{q_\phi(\mathbf{x}|\mathbf{y})} \{\mathbf{X}\mathbf{h}\} + \mathbf{h}^\dagger \mathbb{E}_{q_\phi(\mathbf{x}|\mathbf{y})} \{\mathbf{X}^\dagger \mathbf{X}\} \mathbf{h}, \end{aligned}$$

and

$$\begin{aligned} &\mathbb{E}_{q_\phi(\mathbf{x}|\mathbf{y})} \{\mathbf{X}^\dagger \mathbf{X}\}_{i,j} = \\ &\begin{cases} \mathbb{E}_{q_\phi(\mathbf{x}|\mathbf{y})} \{ (\mathbf{x}^{(L-a)}|\mathbf{x}^{(L-a)}|^{e})^\dagger (\mathbf{x}^{(L-b)}|\mathbf{x}^{(L-b)}|^{f}) \} & a = b \\ \mathbb{E}_{q_\phi(\mathbf{x}|\mathbf{y})} \{ ((\mathbf{x}^{(L-a)}|\mathbf{x}^{(L-a)}|^{e})^\dagger) \\ \quad \times \mathbb{E}_{q_\phi(\mathbf{x}|\mathbf{y})} \{ (\mathbf{x}^{(L-a)}|\mathbf{x}^{(L-a)}|^{f}) \} \} & a \neq b, \end{cases} \end{aligned}$$

where $a, b \equiv i, j \pmod{2L+1}$, $e = \lfloor \frac{i}{2L+1} \rfloor$, and $f = \lfloor \frac{j}{2L+1} \rfloor$.

ACKNOWLEDGMENT

Jinxiang Song greatly appreciates the Ericsson Research Foundation for supporting his research visit to the Communications Engineering Lab (CEL) at Karlsruhe Institute of Technology (KIT), 76131 Karlsruhe, Germany.

REFERENCES

- [1] G. Malik and A. S. Sappal, "Adaptive equalization algorithms: An overview," *Int. J. Adv. Comput. Sci. Appl.*, vol. 2, no. 3, 2011.
- [2] J. C. Cartledge, F. P. Guiomar, F. R. Kschischang, G. Liga, and M. P. Yankov, "Digital signal processing for fiber nonlinearities," *Opt. Express*, vol. 25, no. 3, pp. 1916–1936, 2017.
- [3] S. Qureshi, "Adaptive equalization," *Proc. IEEE*, vol. 73, no. 9, pp. 1349–1387, 1985.
- [4] S. Luo, S. K. O. Soman, L. Lampe, J. Mitra, and C. Li, "Learning for perturbation-based fiber nonlinearity compensation," in *Proc. Eur. Conf. Opt. Commun. (ECOC)*, 2022, p. We1C.4.
- [5] L. Tong, G. Xu, and T. Kailath, "Blind identification and equalization based on second-order statistics: A time domain approach," *IEEE Trans. Inf. Theory*, vol. 40, no. 2, pp. 340–349, 1994.
- [6] J. C. Patra, R. N. Pal, R. Baliarsingh, and G. Panda, "Nonlinear channel equalization for QAM signal constellation using artificial neural networks," *IEEE Trans. Syst., Man, Cybern., B*, vol. 29, no. 2, pp. 262–271, 1999.
- [7] G. Kechriotis, E. Zervas, and E. S. Manolakos, "Using recurrent neural networks for adaptive communication channel equalization," *IEEE Trans. Neural Netw.*, vol. 5, no. 2, pp. 267–278, 1994.
- [8] J. C. Patra, W. C. Chin, P. K. Meher, and G. Chakraborty, "Legendre-FLANN-based nonlinear channel equalization in wireless communication system," in *Proc. IEEE Int. Conf. Syst., Man, Cybern.*, 2008, pp. 1826–1831.
- [9] M. A. Jarajreh *et al.*, "Artificial neural network nonlinear equalizer for coherent optical OFDM," *IEEE Photon. Technol. Lett.*, vol. 27, no. 4, pp. 387–390, 2014.
- [10] D. Jianping, N. Sundararajan, and P. Saratchandran, "Communication channel equalization using complex-valued minimal radial basis function neural networks," *IEEE Trans. Neural Netw.*, vol. 13, no. 3, pp. 687–696, 2002.
- [11] P. J. Freire, J. E. Prilepsky, Y. Osadchuk, S. K. Turitsyn, and V. Aref, "Deep neural network-aided soft-demapping in coherent optical systems: Regression versus classification," *IEEE Trans. Commun.*, vol. 70, no. 12, pp. 7973–7988, 2022.
- [12] P. J. Freire, A. Napoli, B. Spinnler, N. Costa, S. K. Turitsyn, and J. E. Prilepsky, "Neural networks-based equalizers for coherent optical transmission: Caveats and pitfalls," *IEEE J. Sel. Top. Quantum Electron.*, vol. 28, no. 4, pp. 1–23, 2022.
- [13] C. Häger and H. D. Pfister, "Nonlinear interference mitigation via deep neural networks," in *Proc. Opt. Fiber Commun. Conf. (OFC)*, 2018, p. W3A.4.
- [14] S. Zhang *et al.*, "Field and lab experimental demonstration of nonlinear impairment compensation using neural networks," *Nat. Commun.*, vol. 10, no. 1, pp. 1–8, 2019.
- [15] D. Godard, "Self-recovering equalization and carrier tracking in two-dimensional data communication systems," *IEEE Trans. Commun.*, vol. 28, no. 11, pp. 1867–1875, 1980.
- [16] K. N. Oh and Y. O. Chin, "Modified constant modulus algorithm: blind equalization and carrier phase recovery algorithm," in *Proc. IEEE Int. Conf. Commun. (ICC)*, vol. 1, 1995, pp. 498–502.
- [17] J. Yang, J.-J. Werner, and G. A. Dumont, "The multimodulus blind equalization and its generalized algorithms," *IEEE J. Sel. Areas Commun.*, vol. 20, no. 5, pp. 997–1015, 2002.
- [18] D. Wang and D. Wang, "Comparison of nonlinear CMA-criterion-based blind equalizers," in *Proc. IEEE Int. Conf. on Wireless Commun. Netw. and Mobile Comput. (WiCom)*, 2010.
- [19] R. Pandey, "Feedforward neural network for blind equalization with PSK signals," *Neural. Comput. Appl.*, vol. 14, no. 4, pp. 290–298, 2005.
- [20] D. Wang and D. Wang, "Generalized derivation of neural network constant modulus algorithm for blind equalization," in *Proc. IEEE Int. Conf. Wireless Commun., Netw. Mobile Comput.*, 2009.
- [21] T. Pfau, S. Hoffmann, and R. Noé, "Hardware-efficient coherent digital receiver concept with feedforward carrier recovery for M-QAM constellations," *J. Lightw. Technol.*, vol. 27, no. 8, pp. 989–999, 2009.
- [22] R. W. Lucky, "Techniques for adaptive equalization of digital communication systems," *Bell Syst. Tech. J.*, vol. 45, no. 2, pp. 255–286, 1966.
- [23] M. S. Faruk, Y. Mori, C. Zhang, and K. Kikuchi, "Proper polarization demultiplexing in coherent optical receiver using constant modulus algorithm with training mode," in *Proc. Optoelectron. Commun. Conf. (OECC)*, 2010, pp. 768–769.
- [24] S. J. Savory, "Digital coherent optical receivers: Algorithms and subsystems," *IEEE J. Sel. Top. Quantum Electron.*, vol. 16, no. 5, pp. 1164–1179, 2010.
- [25] A. Caciularu and D. Burshtein, "Blind channel equalization using variational autoencoders," in *Proc. IEEE Int. Conf. Commun. Workshops (ICC Workshops)*, 2018.
- [26] —, "Unsupervised linear and nonlinear channel equalization and decoding using variational autoencoders," *IEEE Trans. Cogn. Commun. Netw.*, vol. 6, no. 3, pp. 1003–1018, 2020.
- [27] V. Lauerer, F. Buchali, and L. Schmalen, "Blind equalization and channel estimation in coherent optical communications using variational autoencoders," *IEEE J. Sel. Areas Commun.*, vol. 40, no. 9, pp. 2529–2539, 2022.
- [28] A. Van Den Oord, O. Vinyals *et al.*, "Neural discrete representation learning," *Adv. Neural Inf. Process. Syst. (NIPS)*, vol. 30, 2017.
- [29] Q. Hu, G. Zhang, Z. Qin, Y. Cai, G. Yu, and G. Y. Li, "Robust semantic communications with masked VQ-VAE enabled codebook," *arXiv preprint arXiv:2206.04011*, 2022.
- [30] M. Nemati and J. Choi, "All-in-one: VQ-VAE for end-to-end joint source-channel coding," 2022.
- [31] C. Zhang, J. Bütepage, H. Kjellström, and S. Mandt, "Advances in variational inference," *IEEE Trans. Pattern Anal. Mach. Intell.*, vol. 41, no. 8, pp. 2008–2026, 2018.
- [32] D. P. Kingma and M. Welling, "Auto-encoding variational bayes," *arXiv preprint arXiv:1312.6114*, 2013.
- [33] S. Abdul Samadh, Q. Liu, X. Liu, N. Ghourchian, and M. Allegue, "Indoor localization based on channel state information," in *Proc. IEEE Top. Conf. Wireless Sensors and Sensor Netw. (WiSNeT)*, 2019.
- [34] M. A. Al-Qaness *et al.*, "Channel state information from pure communication to sense and track human motion: A survey," *Sensors*, vol. 19, no. 15, p. 3329, 2019.
- [35] C. Dorize, S. Guerrier, E. Awwad, and J. Renaudier, "Capturing acoustic speech signals with coherent MIMO phase-OTDR," in *Proc. Eur. Conf. Opt. Commun. (ECOC)*, 2020.

- [36] R. J. Williams, "Simple statistical gradient-following algorithms for connectionist reinforcement learning," *Machine learning*, vol. 8, no. 3, pp. 229–256, 1992.
- [37] C. Karras, A. Karras, M. Avlonitis, and S. Sioutas, "An overview of MCMC methods: from theory to applications," in *Proc. Int. Conf. on Artificial Intell. Appl. Innov.* Springer, 2022, pp. 319–332.
- [38] Y. Bengio, N. Léonard, and A. Courville, "Estimating or propagating gradients through stochastic neurons for conditional computation," *arXiv preprint arXiv:1308.3432*, 2013.
- [39] J. Lucas, G. Tucker, R. B. Grosse, and M. Norouzi, "Don't blame the ELBO! A linear VAE perspective on posterior collapse," *Adv. Neural Inf. Process. Syst. (NeurIPS)*, vol. 32, 2019.
- [40] D. P. Kingma and J. Ba, "Adam: A method for stochastic optimization," *arXiv preprint arXiv:1412.6980*, 2014.
- [41] L. Schmalen, A. Alvarado, and R. Rios-Müller, "Performance prediction of nonbinary forward error correction in optical transmission experiments," *J. Lightw. Technol.*, vol. 35, no. 4, pp. 1015–1027, 2017.
- [42] D. E. Crivelli *et al.*, "Architecture of a single-chip 50 Gb/s DP-QPSK/BPSK transceiver with electronic dispersion compensation for coherent optical channels," *IEEE Trans. Circuits Syst. I, Reg. Papers*, vol. 61, no. 4, pp. 1012–1025, 2014.
- [43] N. Kaneda and A. Leven, "Coherent polarization-division-multiplexed QPSK receiver with fractionally spaced CMA for PMD compensation," *IEEE Photon. Technol. Lett.*, vol. 21, no. 4, pp. 203–205, 2009.
- [44] S. Goossens *et al.*, "Introducing 4d geometric shell shaping for mitigating nonlinear interference noise," *J. Lightw. Technol.*, vol. 41, no. 2, pp. 599–609, 2023.
- [45] *Implementation agreement 400ZR*, OIF-400ZR-01.0, Optical Internet-working Forum, Mar. 2020. [Online]. Available: https://www.oiforum.com/wp-content/uploads/OIF-400ZR-01.0_reduced2.pdf
- [46] V. Bajaj, F. Buchali, M. Chagnon, S. Wahls, and V. Aref, "Deep neural network-based digital pre-distortion for high baudrate optical coherent transmission," *J. of Lightw. Technol.*, vol. 40, no. 3, pp. 597–606, 2022.
- [47] Y. Wu, U. Gustavsson, A. Graell i Amat, and H. Wymeersch, "Low complexity joint impairment mitigation of I/Q modulator and PA using neural networks," *IEEE J. Sel. Areas Commun.*, vol. 40, no. 1, pp. 54–64, 2021.
- [48] X. Cheng, D. Liu, Z. Zhu, W. Shi, and Y. Li, "A ResNet-DNN based channel estimation and equalization scheme in FBMC/OQAM systems," in *Proc. IEEE Int. Conf. on Wireless Commun. Signal Proc. (WCSP)*, 2018.
- [49] D. R. Morgan, Z. Ma, J. Kim, M. G. Zierdt, and J. Pastalan, "A generalized memory polynomial model for digital predistortion of RF power amplifiers," *IEEE Trans. Signal Proc.*, vol. 54, no. 10, pp. 3852–3860, 2006.
- [50] V. Kamalov *et al.*, "Evolution from 8QAM live traffic to PS 64-QAM with neural-network based nonlinearity compensation on 11000 km open subsea cable," in *Proc. Opt. Fiber Commun. Conf. (OFC)*, 2018, p. Th4D.5.
- [51] F. Diedolo, G. Böcherer, M. Schädler, and S. Calabró, "Nonlinear equalization for optical communications based on entropy-regularized mean square error," in *Proc. Eur. Conf. Opt. Commun. (ECOC)*, 2022, p. We2C.2.
- [52] J. Kim and K. Konstantinou, "Digital predistortion of wideband signals based on power amplifier model with memory," *Electron. Lett.*, vol. 37, no. 23, p. 1, 2001.
- [53] X. Liu *et al.*, "Beam-oriented digital predistortion for 5G massive MIMO hybrid beamforming transmitters," *IEEE Trans. Microw. Theory Tech.*, vol. 66, no. 7, pp. 3419–3432, 2018.
- [54] Y. Wu, J. Song, C. Häger, U. Gustavsson, A. Graell i Amat, and H. Wymeersch, "Symbol-based over-the-air digital predistortion using reinforcement learning," in *Proc. Int. Conf. Commun. (ICC)*, 2022, pp. 2615–2620.
- [55] G. Paryanti, H. Faig, L. Rokach, and D. Sadot, "A direct learning approach for neural network based pre-distortion for coherent nonlinear optical transmitter," *J. Lightw. Technol.*, vol. 38, no. 15, pp. 3883–3896, 2020.